spectroscopy journal

MDPI

Article

Towards Fast Quantum Cascade Laser Spectrometers for High-Throughput and Cost-Effective Disease Surveillance

Mauro Pazmiño-Betancourth [1,*], Aleksandr Boldin [2], Victor Ochoa-Gutierrez [3], Richard A. Hogg [4], Francesco Baldini [1,5], Mario González-Jiménez [6], Klaas Wynne [6] and David Childs [7]

1 School of Biodiversity, One Health and Veterinary Medicine, University of Glasgow, Glasgow G12 8QQ, UK; francesco.baldini@gasgow.ac.uk
2 James Watt School of Engineering, University of Glasgow, Glasgow G12 8QQ, UK; a.boldin.1@research.gla.ac.uk
3 Jacobs Technion-Cornell Institute, Cornell Tech, New York, NY 10044, USA; victorog@cornell.edu
4 Aston Institute of Photonic Technologies (AiPT), College of Engineering and Physical Sciences, Birmingham B4 7ET, UK; r.hogg1@aston.ac.uk
5 Environmental Health and Ecological Sciences Department, Ifakara Health Institute, Morogoro P.O. Box 53, Tanzania
6 School of Chemistry, University of Glasgow, Glasgow G12 8QQ, UK; mario.gonzalezjimenez@glasgow.ac.uk (M.G.-J.); klaas.wynne@glasgow.ac.uk (K.W.)
7 Huawei Technologies R&D UK Ltd., Huawei, Ipswich IP5 3RE, UK; davidchilds8@gmail.com
* Correspondence: mauro.pazminobetancourth@glasgow.ac.uk

Abstract: Fourier transform infrared (FTIR) spectroscopy, coupled with machine learning (ML) analysis can be used for disease monitoring with high speed and accuracy, including the classification of mosquito samples by species, age and malaria detection. However, current FTIR instruments use low-brightness thermal light sources to generate infrared light, which limits their ability to measure complex biological samples, especially where high spatial resolution is necessary, such as for specific mosquito tissues. Moreover, these systems lack portability, which is essential for field applications. To overcome these issues, spectrometers using quantum cascade lasers (QCLs) have become an attractive alternative for building fast, and portable systems due to their high electrical-to-optical efficiency, small size, and potential for low-cost. Here, we present a QCL-based spectrometer prototype designed for large scale, low-cost, environmental field-based disease surveillance.

Keywords: quantum cascade lasers; infrared; spectroscopy; anopheles; malaria

Academic Editor: Clemens Burda

Received: 5 February 2025
Revised: 4 March 2025
Accepted: 5 March 2025
Published: 7 March 2025

Citation: Pazmiño-Betancourth, M.; Boldin, A.; Ochoa-Gutierrez, V.; Hogg, R.A.; Baldini, F.; González-Jiménez, M.; Wynne, K.; Childs, D. Towards Fast Quantum Cascade Laser Spectrometers for High-Throughput and Cost-Effective Disease Surveillance. *Spectrosc. J.* **2025**, *3*, 8. https://doi.org/10.3390/spectroscj3010008

1. Introduction

Infrared spectroscopy is one of the most important and versatile techniques for chemical analysis. It characterises not only the chemical composition of a sample, but also the structural properties of its molecules by measuring the absorption of light by exciting its chemical bonds. This is possible thanks to functional groups absorbing infrared radiation due to changes in the dipole moment during the vibration of molecules within the sample [1]. Infrared spectroscopy probes these vibrational modes [2] whose frequency depends on the strength of the bonds and the mass of the atoms involved [3]. Every different functional group absorbs at a different frequency, so an absorption spectrum of a biological sample contains a set of unique absorption signatures indicating the presence of proteins, carbohydrates, lipids, and nucleic acids [4].

Fourier transform infrared spectrometers (FTIR) are the industry standard for mid-infrared spectroscopy across a variety of areas and applications [5]. They traditionally use Globars (silicon carbide rods) as a light source since they emit broadband radiation, but

this incoherent source and the large optics necessary for reasonable collimation do not allow for compact systems or high-resolution microscopy without significant loss of signal-to-noise ratio. Nonetheless, the usefulness of mid-infrared spectroscopy for mosquito surveillance [6] and malaria diagnosis [7] using FTIR have shown promising results in laboratory and field settings [8,9]. Several drawbacks in this application are; its infrared light is emitted with a low brightness, which can limit its use with high absorbance samples such as mosquitoes [10]. It also lacks spatial coherence and often requires liquid nitrogen cooled HgCdTe (MCT) detectors to achieve sufficient signal-to-noise ratio [11]. Lastly, the presence of an interferometer limits the miniaturisation of FTIR equipment for field applications [12,13]. Even though, FTIR spectrometers based on micro-electrotechnical systems (MEMS) have reported resolutions of 8 cm^{-1}, repeatability and reliability issues are still present which prevent their commercial use [14].

Since Quantum Cascade Lasers (QCL) were demonstrated in 1994 [15], they have already challenged conventional FTIR thanks to the advances in QCL performance at room temperature, namely in power output, gain bandwidth and wall-plug efficiency [16]. They offer compactness [17], high optical output power [18], comparable SNR to FTIR when using non-cryogenic thermoelectrically cooled detectors and faster spectral data acquisition [19]. Numerous studies have reported an increase in speed and resolution in chemical imaging [20], and specifically improved analysis of the amide I and II bands in proteins [21]. QCL technology is fundamental to fill the gaps in hardware development of portable and fast systems in disease and vector surveillance [22–24].

As supporting evidence for mid-infrared spectroscopy as a reliable tool for disease surveillance is increasing, it is timely to explore alternatives to FTIR to adapt it to the challenges in field deployment. We need to build compact and field-ready systems that can be deployed anywhere in the world due to the global prevalence of vector-borne diseases. Building on current developments in room-temperature operating continuous-wave QCLs, here we build and evaluate a compact spectrometer using an external Cavity (EC) QCL-based spectrometer in the 9–10.5 µm MIR region.

2. Materials and Methods

Laser and External Cavity Configuration

Figure 1 shows the optical cavity configuration of our laser setup. The Littman-Metcalf type external cavity configuration consists of four main elements: The gain element (optical amplifier), in this case a quantum cascade (QC) chip with high reflection back facet and antireflection coated front facet to avoid Fabry-Perot lasing. Light is collimated by a high numerical aperture antireflection coated chalcogenide lens (6.55 mm diameter, EFL = 4.0 mm, with an 8 to 12 µm AR coating on both surfaces) before wavelength selection by a diffraction grating and a scanning galvanometer mirror. The QC chip is AuSn soldered to an aluminium nitride (AlN) carrier, custom-made (Thorlabs Quantum Electronics, Newton, NJ, USA) and the carrier is mounted on a copper heat-spreader and stabilised with a thermoelectric cooler. The resulting heat from the thermoelectric cooler is removed to the ambient lab environment. This system is more compact than a traditional chiller and offers an additional advantage of allowing cooling down to −30 °C, if necessary. The collimated beam from the laser is rotated in polarisation by the two unprotected gold coated mirrors (m1 and m2) and directed onto a diffraction grating (100 grooves/mm blazed for a wavelength of 10.6 µm). This change in polarisation is carried out because of the highest efficiency of the grating is the orthogonal polarisation to the laser emission. From the grating, a single wavelength within the first diffraction order is selected by the angle of the galvanometer driven mirror and reflected back to the diffraction grating. Wavelength selection and feedback to the QCL gain chip is therefore controlled by the rotation angle of the galvanometer

mounted mirror. Lasing is achieved so long as the cavity losses are less than the gain of the QC gain chip. Light is extracted from the cavity in the zeroth order reflection from the diffraction grating. The scanning galvanometer mirror is lightweight, and therefore wavelength selection can occur through fast sweeping. This cavity configuration is chosen for simplicity of adaptation and ensures that the output beam does not move in angle, such that a sample scanning and microscopy stage can be easily incorporated. A second benefit is that the double pass on the grating decreases the bandwidth of the external cavity and so decreases the instantaneous laser spectrum of the laser, for higher spectral resolution. For a given resolution, this allows a route to shrink the beam size and so grating size to be more compact than an equivalent Littrow configuration. The galvanometer was a GVS111, 1D large beam (10 mm) diameter galvo system with a servo driver board (Thorlabs, Ely, UK). The mirror swings by 0.8° per volt applied from a digital to analogue converter card. The encoder feedback channel from the mirror position is captured by the analogue to digital converter on the same card, along with the detector signal. The detector used was an amplified HgCdTe (MCT) photovoltaic detector (2.0–10.6 m, Thorlabs, UK). It has an integrated hyper-hemispherical GaAs lens for optical immersion and a wedged ZnSe window AR-coated for 2–13 µm. All analogue signals from the system are connected to a desktop computer via a DAQ PCIe card (PCIE 1802-AE, Advantech Ltd., London, UK). This card is a combined multi-channel digital to analogue converter (DAC) and analogue to digital converter (ADC). The inputs are the detector signal and the galvanometer position, while the analogue signals out of the system are a waveform to the servo driver of the galvo system. The power supply for the laser and thermoelectric cooler is the ITC-4001QCL bench-top laser diode and temperature controller (Thorlabs, UK). The power source for the galvanometer is the GPS011-EC galvo system linear power supply (Thorlabs, UK). The system is controlled by custom-made LabVIEW programs.

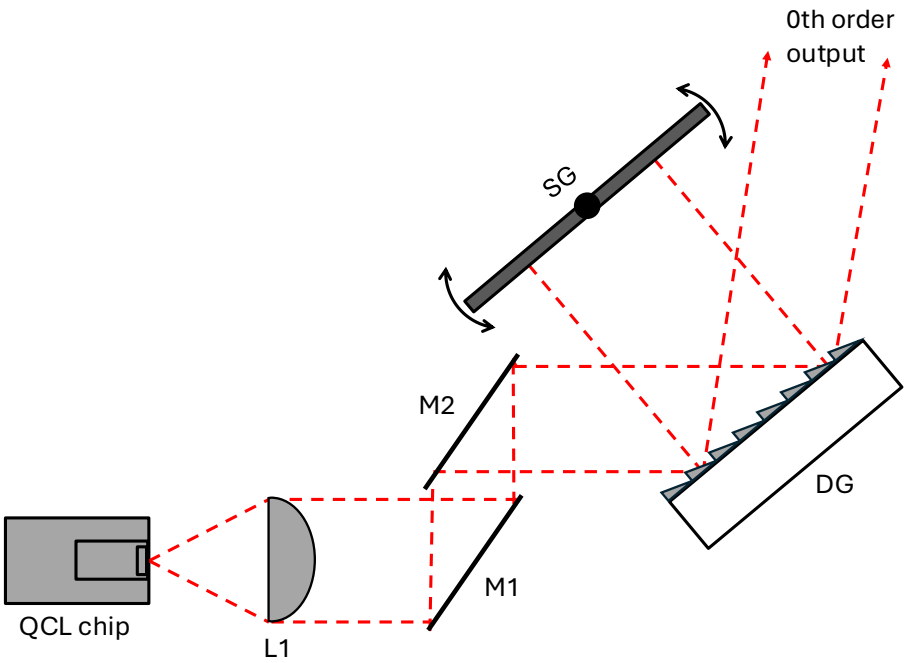

Figure 1. Diagram of the external cavity in Littman-Metcalf configuration. The tuning element is a galvanometer scanning mirror, combined with a fixed diffraction grating. Infrared radiation can be extracted from the zeroth-order diffracted light from the grating. QCL: quantum cascade amplifier chip with HR coated back facet. L1: collimating lens. M1, 2: gold-coated polarisation rotation mirrors.: DG: diffraction grating. SG: scanning galvanometer.

3. Results

3.1. EC-QCL Spectral Characterization

The spectral characterisation of our QCL system was performed with an FTIR (vertex 70 v, Bruker, Billerica, MA, USA) with a deuterated triglycine sulphate (DTGS) detector using 32 scans with a resolution of 0.3 cm^{-1}. The emission spectra of the EC-QCL system were measured at different galvanometer angles with a current injection of 1.7 A in continuous wave (CW) operation. The wavenumber of the laser can be tuned over approximately 140 cm^{-1}, from 960 cm^{-1} to 1100 cm^{-1} (Figure 2a). The maximum optical output power was 12 mW at 1049 cm^{-1} and output power follows the spectral profile (Figure 2b) of the QC gain chip. Instantaneous linewidth measured by the FTIR is 0.3 cm^{-1}, limited by the FTIR resolution, and was constant across the tuning range of the laser (Figure 2c). The tuning linearity between peak emission wavelength and grating position is shown in Figure 2d.

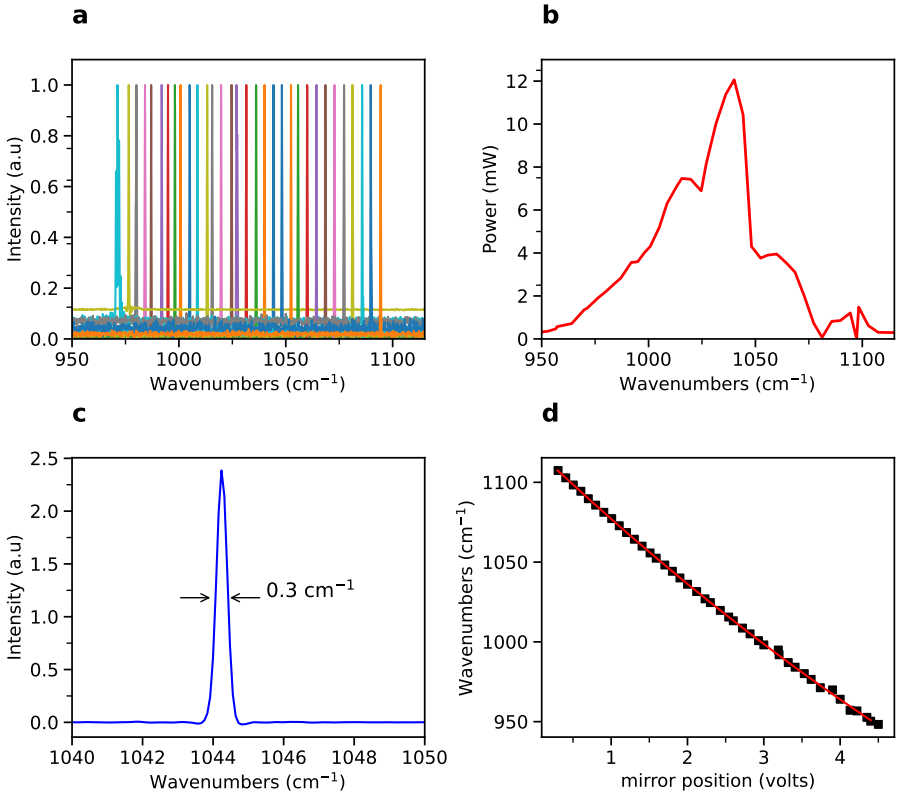

Figure 2. (**a**) Normalised emission lines of the EC−QCL during the wavenumber scan. Each measurement was collected by rotating the scanning galvanometer mirror by 0.1 v. Each colour represents a different position of the mirror. Current injection of 1.7 A. (**b**) Measured CW output power of the EC-QCL as a function of wavenumber. The maximum power peak of 12.6 mW was achieved at 1040 cm^{-1}. (**c**) Laser spectrum of the EC-QCL at the wavenumber of 1044.3 cm^{-1} with a linewidth of 0.3 cm^{-1}. (**d**) Step-scan measurements of emission spectrum of the EC- QCL during a scan between 950 to 1100 cm^{-1} recorded with 0.3 cm^{-1} spectral resolution.

3.2. Processing EC-QCL Data

Initially, one hundred scans were collected to establish the 'background' followed by the sample measurement, where each scan consisted of 1000 data points. The QCL beam was aimed to the same position when measuring backgrounds and samples by using a sample holder. The background (I_o) and sample (I) scans were averaged independently using ensembled averaging. Final transmittance was calculated with the average spectra from the background and sample using Equation (1). Fresh background measurements

were taken every time a sample was measured. Gaussian filters for smoothing the signal and Saviztky-Golay for second derivatives were applied to the final transmittance. The absorbance was calculated using the negative logarithm of the transmittance (Equation (2)). All pre-processing and analysis were performed using Python 3.10 with in-house scripts.

$$T = \frac{I}{I_o} \tag{1}$$

$$A = -log_{10}T \tag{2}$$

3.3. Speed Characterization

To assess the spectroscopic capabilities of our system at different scanning speeds, absorption spectra were measured from a calibrated sample made of 0.3 µm thick polystyrene (PS) with characteristic absorption bands located at 1028 cm^{-1} and 1068 cm^{-1}. A triangular wave output from the data acquisition card at different frequencies ranging from 127 to 500 Hz was used to drive the galvo-mirror in a linear scan through the lasing tuning range and back again. Spectral measurements were co-added for an average of 100 scans for each, background, and sample measurements, with a total acquisition time of 2 s per sample at 127 Hz decreasing to 0.8 s at 500 Hz. Each measurement consisted of 1000 data points separated by ≈0.3 cm^{-1}. The two main PS absorption bands at 1028 and 1069 cm^{-1} can be seen at all scan speeds (Figure 3). Spectra show high correlation between scan rates, however, there is a slight shift at faster scanning speeds. The largest shift occurs at 500 Hz of ≈1.2 cm^{-1} when compared to the 127 Hz due to the lag introduced by the rise and fall time of the pyro-electric sensor and the changing signal intensity. Laser range was also affected by frequency scans, as expected, since the moving mass of the mirror is unable to reach larger deflection angles with a fixed input power limit to the galvo motor. The range reduced from the static range of 135 cm^{-1} to 80 cm^{-1} at 500 Hz (Figure 3). The spectrum also shows noise in the 1050 to 1100 cm^{-1} region. This is caused by the lower optical power of the laser, which decreases the signal-to-noise ratio.

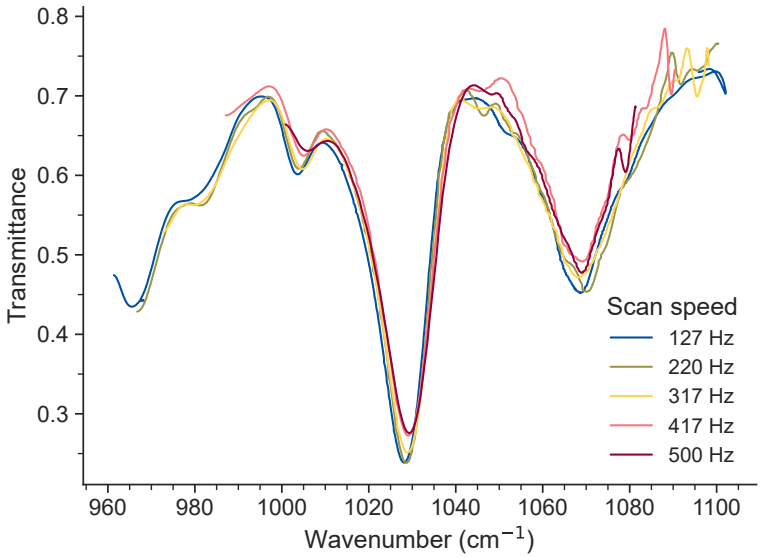

Figure 3. Mid-infrared spectroscopy measurements of Polystyrene (PS) at different scanning speeds. Each coloured line represents a scan speed, ranging from 127 Hz to 500 Hz.

3.4. Application on Biological Samples

Mid-IR transmission spectra of *Anopheles gambiae* (Kisumu strain) mosquitoes were recorded using the fast-swept mode. A spectrum was acquired by continuously tuning the galvanometer over the full spectral range (950–1100 cm^{-1}) at a tuning rate of 127 Hz and

an instantaneous spectral resolution of 0.3 cm^{-1}. The mosquito samples were processed using the KBr disc method for transmission measurements. First, the mosquitoes were stored in universal tubes with silica gel at 4 °C for at least three days to eliminate their water content [6]. Then, the sample was ground with KBr powder using a simple mortar and pestle made of agate, small enough to minimise infrared light scattering. The resulting mixture was then compacted in a press until a translucent disc was obtained. This facilitates transmission measurements from what would otherwise be too thick a sample for light to pass through with measurable absorption. One hundred scans per spectrum were averaged for each background (a KBr disc without a sample), and sample, for a total acquisition time of ≈3 s. After data collection, a Savitzky-Golay second derivative was applied to the final spectrum. To generate the spectrum using FTIR, the same sample and background were measured using a dry-air purged Bruker Vertex 70 spectrometer (Bruker Corporation, Billerica, MA, USA) equipped with a Globar lamp, a Deuterated Lanthanum α-lanine doped TriGlycine Sulphate (DLaTGS) detector, a potassium bromide (KBr) beamsplitter in transmission mode with 4 cm^{-1} resolution. Comparison between FTIR and EC-QCL second derivative spectra found agreement with three out of the four absorption bands. The band at 1056 is not well resolved in the EC-QCL spectrum (Figure 4). Three absorption bands were identified at 988, 1029, and 1056 cm^{-1}. Band 1029 is related to chitin (Table 1). The shape of the raw spectrum is comparable with the FTIR; however, baseline shifts in the 1050–1100 cm^{-1} region are observed. In comparison, between the second derivative spectra, there is an agreement between bands, however, the artefacts of the spectrum from the EC-QCL are amplified by the second derivative method.

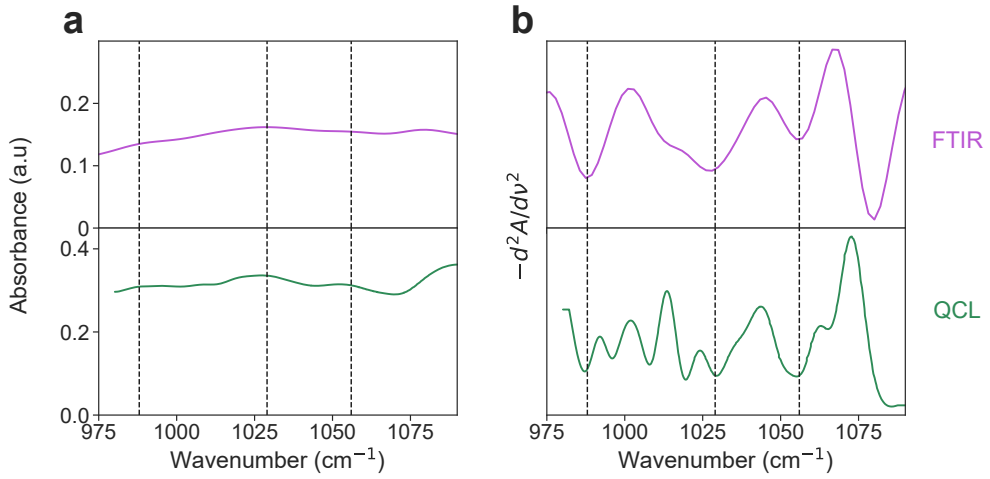

Figure 4. Mid infrared spectra of an *Anopheles gambiae* mosquito recorded with the EC-QCL setup (green line) and with a commercial FTIR (purple line) as (**a**) absorbance vs. wavenumber values and as (**b**) second derivative vs wavenumber values. Black dashed lines show the agreement of the spectral features between the two systems.

Table 1. Assignment of wavenumber values found and tentative band assignments in the mosquito sample using the EC-QCL prototype.

Wavenumber (cm^{-1})	Band Assignment	Compound
988	–	–
1029	C-O	Chitin
1056	C-O	–

4. Discussion

Infrared spectroscopy has become an attractive technique to use in vector-borne diseases surveillance. However, current commercial FTIR machines are not suitable for

the required field work. Quantum Cascade Laser based spectrometers are flexible and powerful enough for the development of custom spectrometers that can accelerate the uptake of spectroscopy to in-routine surveillance.

Here, we have demonstrated the use of our custom-built EC-QCL to acquire spectra from *An. gambiae* mosquitoes. Our current set up can measure mosquito samples using transmission in the 950–1100 cm^{-1} region in ≈3 s. The functional groups assigned to this region are C–O–C and C–O stretch [25]. Previous works have shown complex set of spectral changes in that region that can be used for malaria diagnosis in mosquitoes and humans [8]. Moreover, we found three matching bands when compared to spectrum collected with a commercial FTIR, specifically a peak at 1029 cm^{-1} related to chitin. It has been described that changes in the absorption of specific wavenumbers related to chitin, wax and proteins from the cuticle using FTIR can be used to predict species and age in mosquitoes [25,26]. Even though we found some agreement between the spectra collected by FTIR and our system, the overall performance of the system will be analysed on how accurate our machine learning models perform on surveillance when using data from the EC-QCL system.

We found some aberrations in the spectra collected with our system, which we attribute to the uneven laser power density across the sample due to the high spatial resolution of a coherent laser source relative to the incoherent source from the FTIR. Also, technical noise from the source driving the laser and the high resolution might increase the overall noise in the signal. Moreover, when using Savitzky-Golay second derivative, small deviations can produce boundary artifacts and enhance high frequency noise [27]. This can be improved in a future version by optimising the power density of the laser to achieve a more Gaussian shape across a more suitable spot size, i.e., without tightly focusing the laser onto the sample disc.

Processing the sample into a KBr disc increases sample throughput time and measurement duration by more than 5 min per sample. We chose to process the sample with KBr due to the mosquito's thickness and the fact that the system currently performs measurements in transmission mode only, which is the easiest to assemble and test, as opposed to diffuse reflectance mode or Attenuated Total Reflection (ATR). However, QCLs can be easily adapted for diffuse reflectance in applications such as the analysis of pharmaceutical formulations [28,29]. Attenuated Total Reflection is used for mosquito age grading and malaria surveillance because it can handle thick samples without any preprocessing, and QCLs can be easily implemented in ATR systems, as shown in studies for glucose monitoring [30–32] and microplastic identification [33].

The range of our system is quite small compared to the 400–4000 cm^{-1} range of commercial FTIR and quite challenging to use due to low absorption of the bands. Machine learning models are good at using tabular data for classification problems as spectral data are fed into these models as absorbance at specific wavenumbers. However, not all the mid-infrared region is needed for this application. The region of 2500–1800 cm^{-1} does not contain biological-related information, which is discarded before analysis. Moreover, species identification in *Aedes* has been carried out using only the region from 1800 to 600 cm^{-1} [25], as well as for prediction of species, age and insecticide status in *Anopheles* [34]. In malaria diagnosis from blood samples, most of the important features used by models to identify malaria parasites were located at 800 to 1100 cm^{-1} [7]. Even though the limited range of the QCLs can be seen as a disadvantage for general lab use, in this use case especially when applied in the field, the fact that the full spectrum does not have to be recorded makes QCL systems more efficient and faster than FTIR. This benefits not only for large volumes of spectral collection but also for future applications such as chemical imaging. If a broader spectral range is needed, gain chips with multiple-stage hetero-cascading active

regions, can increase the spectral range to 772 cm^{-1} [35]. Also, multiple QCL gain chips with different wavelength ranges can be combined, extending the range, or using specific sections of the spectrum accordingly to specific needs. Commercial systems have up to 4 gain chips providing coverage of 5.4 to 12.8 microns (800 to 1800 cm^{-1}) or wider in pulsed operation, and similar ranges in CW [36].

As evidence of the use of FTIR in field settings for age grading and malaria diagnosis increases, the translation of this technology will depend on how well infrared data can predict biological traits in field settings, the costs of manufacture, and how the system can be implemented into already established routine surveillance workflows. There is a need to validate the predictive power of infrared spectroscopy in field settings, which will neeed to be addressed [23]. Regarding implementation costs, our setup costs around £18,000 to build with off-the-shelf components. As we optimise future iterations of this setup and as technology uptake increases, chip costs will decrease, making the whole system more affordable. Fourier Transform IR spectrometers with QCL lasers are being commercialised from major companies such as Bruker, indicating that the market has a demand for this type of technology. Additionally, the increasing number of publications testing other vibrational spectroscopy techniques, such as Raman [37,38] to overcome current drawbacks of traditional techniques for vector/disease surveillance further highlights the need for device development. Finally, adapting this technology to routine surveillance will require equipment acquisition and staff training; however, it can vastly reduce data acquisition time and increase the amount of data that can be collected to improve disease surveillance. Therefore, EC-QCL has great potential for vector and disease surveillance due to its versatility and adaptability.

5. Conclusions

We have demonstrated the use of a fast swept continuous wave EC-QCL system for mid-IR spectroscopy in mosquito samples in the 950–1100 cm^{-1} region. In summary: (i) High speed and high tuning rate were achieved using off-the-shelf optical components, which also means that there is room for future optimisation. (ii) The system can collect spectral information from whole *An. gambiae* mosquitoes processed in KBr discs at speeds of 100 spectra per second with little optimisation. (iii) Absorption bands in the spectrum from mosquitoes matched their position when compared with a commercial FTIR spectrometer. (iv) The current prototype has the potential for extreme miniaturisation and a lower cost for its use in the field.

Author Contributions: Conceptualization, D.C. and M.P.-B.; methodology, D.C. and M.P.-B.; software, M.P.-B. and A.B.; validation, M.P.-B., V.O.-G. and M.G.-J.; formal analysis, M.P.-B.; investigation, M.P.-B. and A.B.; resources, D.C and M.G.-J.; data curation, M.P.-B. and V.O.-G.; writing—original draft preparation, M.P.-B.; writing—review and editing, M.P.-B., V.O.-G., R.A.H., F.B., M.G.-J., K.W. and D.C.; visualization, M.P.-B.; supervision, D.C., F.B. and K.W.; project administration, D.C. and F.B.; funding acquisition, D.C., F.B. and K.W. All authors have read and agreed to the published version of the manuscript.

Funding: M.P.-B. was supported by the Lord Kelvin Adam Smith studentship from the University of Glasgow and Research Incentive Grant 2024. F.B. were supported by the Medical Research Council (MRC) grant (Grant No. MR/P025501/1), the Bill and Melinda Gates Foundation (grant number Grant No. OPP 1217647 to Ifakara Health Institute). F.B. was supported by the Academy Medical Sciences Springboard Award (Ref: SBF007\100094).

Institutional Review Board Statement: Not applicable.

Informed Consent Statement: Not applicable.

Data Availability Statement: The original data presented in the study are openly available in Enlighten repository at https://researchdata.gla.ac.uk/1173/ (accessed on 4 February 2025). The code for reproducing the figures can be accessed at https://github.com/maurocolapso/QCL_Pazminoetal (accessed on 4 February 2025).

Acknowledgments: We would like to thank Matthew Steer for invaluable advice on characterisation of the laser.

Conflicts of Interest: Author David Childs was employed by the company Huawei. The remaining authors declare that the research was conducted in the absence of any commercial or financial relationships that could be construed as a potential conflict of interest.

References

1. Ng, L.M.; Simmons, R. Infrared Spectroscopy. *Anal. Chem.* **1999**, *71*, 343–350. [CrossRef]
2. Stuart, B.H. *Infrared Spectroscopy: Fundamentals and Applications*; John Wiley & Sons, Inc.: Hoboken, NJ, USA, 2004; Volume 8.
3. Smith, B. *Infrared Spectral Interpretation: A Systematic Approach*; CRC Press: Boca Raton, FL, USA, 2018.
4. Baker, M.J.; Trevisan, J.; Bassan, P.; Bhargava, R.; Butler, H.J.; Dorling, K.M.; Fielden, P.R.; Fogarty, S.W.; Fullwood, N.J.; Heys, K.A.; et al. Using Fourier transform IR spectroscopy to analyze biological materials. *Nat. Protoc.* **2014**, *9*, 1771–1791. [CrossRef] [PubMed]
5. Isensee, K.; Kröger-Lui, N.; Petrich, W. Biomedical applications of mid-infrared quantum cascade lasers—A review. *Analyst* **2018**, *143*, 5888–5911. [CrossRef]
6. González Jiménez, M.; Babayan, S.A.; Khazaeli, P.; Doyle, M.; Walton, F.; Reedy, E.; Glew, T.; Viana, M.; Ranford-Cartwright, L.; Niang, A.; et al. Prediction of mosquito species and population age structure using mid-infrared spectroscopy and supervised machine learning [version 3; peer review: 2 approved]. *Wellcome Open Res.* **2019**, *4*, 76. [CrossRef]
7. Mwanga, E.P.; Minja, E.G.; Mrimi, E.; Jiménez, M.G.; Swai, J.K.; Abbasi, S.; Ngowo, H.S.; Siria, D.J.; Mapua, S.; Stica, C.; et al. Detection of malaria parasites in dried human blood spots using mid-infrared spectroscopy and logistic regression analysis. *Malar. J.* **2019**, *18*, 341. [CrossRef] [PubMed] [PubMed Central]
8. Mwanga, E.P.; Mchola, I.S.; Makala, F.E.; Mshani, I.H.; Siria, D.J.; Mwinyi, S.H.; Abbasi, S.; Seleman, G.; Mgaya, J.N.; Jiménez, M.G.; et al. Rapid assessment of the blood-feeding histories of wild-caught malaria mosquitoes using mid-infrared spectroscopy and machine learning. *Malar. J.* **2024**, *23*, 86. [CrossRef]
9. Siria, D.J.; Sanou, R.; Mitton, J.; Mwanga, E.P.; Niang, A.; Sare, I.; Johnson, P.C.; Foster, G.M.; Belem, A.M.; Wynne, K.; et al. Rapid age-grading and species identification of natural mosquitoes for malaria surveillance. *Nat. Commun.* **2022**, *13*, 1–9. [CrossRef] [PubMed]
10. Akhgar, C.K.; Ramer, G.; Żbik, M.; Trajnerowicz, A.; Pawluczyk, J.; Schwaighofer, A.; Lendl, B. The Next Generation of IR Spectroscopy: EC-QCL-Based Mid-IR Transmission Spectroscopy of Proteins with Balanced Detection. *Anal. Chem.* **2020**, *92*, 9901–9907. [CrossRef]
11. Ogunleke, A.; Bobroff, V.; Chen, H.H.; Rowlette, J.; Delugin, M.; Recur, B.; Hwu, Y.; Petibois, C. Fourier-transform vs. quantum-cascade-laser infrared microscopes for histo-pathology: From lab to hospital? *TrAC Trends Anal. Chem.* **2017**, *89*, 190–196. [CrossRef]
12. Erfan, M.; Sabry, Y.M.; Mortada, B.; Sharaf, K.; Khalil, D. Mid infrared MEMS FTIR spectrometer. In Proceedings of the MOEMS and Miniaturized Systems XV, San Francisco, CA, USA, 15–17 February 2016; Volume 9760, pp. 103–109.
13. Koyama, T.; Kino, S.; Matsuura, Y. Accuracy improvement of blood glucose measurement system using quantum cascade lasers. *Opt. Photonics J.* **2019**, *9*, 155. [CrossRef]
14. Chai, J.; Zhang, K.; Xue, Y.; Liu, W.; Chen, T.; Lu, Y.; Zhao, G. Review of MEMS Based Fourier Transform Spectrometers. *Micromachines* **2020**, *11*, 214. [CrossRef] [PubMed]
15. Faist, J.; Capasso, F.; Sivco, D.L.; Sirtori, C.; Hutchinson, A.L.; Cho, A.Y. Quantum cascade laser. *Science* **1994**, *264*, 553–556. [CrossRef] [PubMed]
16. Rassel, S.; Xu, C.; Zhang, S.; Ban, D. Noninvasive blood glucose detection using a quantum cascade laser. *Analyst* **2020**, *145*, 2441–2456. [CrossRef] [PubMed]
17. Tuzson, B.; Graf, M.; Ravelid, J.; Scheidegger, P.; Kupferschmid, A.; Looser, H.; Paulo Morales, R.; Emmenegger, L. A compact QCL spectrometer for mobile, high-precision methane sensing aboard drones. *Atmos. Meas. Tech.* **2020**, *13*, 4715–4726. [CrossRef]
18. Delbeck, S.; Heise, H.M. FT-IR versus EC-QCL spectroscopy for biopharmaceutical quality assessment with focus on insulin—Total protein assay and secondary structure analysis using attenuated total reflection. *Anal. Bioanal. Chem.* **2020**, *412*, 4647–4658. [CrossRef] [PubMed]

19. Schwaighofer, A.; Alcaráz, M.R.; Araman, C.; Goicoechea, H.; Lendl, B. External cavity-quantum cascade laser infrared spectroscopy for secondary structure analysis of proteins at low concentrations. *Sci. Rep.* **2016**, *6*, 33556. [CrossRef]
20. Kuepper, C.; Kallenb, A.; Juette, H.; Tannapfel, A.; Großerueschkamp, F.; Gerwert, K.; Kallenbach-Thieltges, A.; Juette, H.; Tannapfel, A.; Großerueschkamp, F.; et al. Quantum Cascade Laser-Based Infrared Microscopy for Label-Free and Automated Cancer Classification in Tissue Sections. *Sci. Rep.* **2018**, *8*, 7717. [CrossRef]
21. Schwaighofer, A.; Akhgar, C.K.; Lendl, B. Broadband laser-based mid-IR spectroscopy for analysis of proteins and monitoring of enzyme activity. *Spectrochim. Acta Part A Mol. Biomol. Spectrosc.* **2021**, *253*, 119563. [CrossRef] [PubMed]
22. Abramov, P.I.; Kuznetsov, E.V.; Skvortsov, L.A.; Skvortsova, M.I. Quantum-Cascade Lasers in Medicine and Biology (Review). *J. Appl. Spectrosc.* **2019**, *86*, 1–26. [CrossRef]
23. Mshani, I.H.; Siria, D.J.; Mwanga, E.P.; Sow, B.B.; Sanou, R.; Opiyo, M.; Sikulu-Lord, M.T.; Ferguson, H.M.; Diabate, A.; Wynne, K.; et al. Key considerations, target product profiles, and research gaps in the application of infrared spectroscopy and artificial intelligence for malaria surveillance and diagnosis. *Malar. J.* **2023**, *22*, 346. [CrossRef]
24. Schwaighofer, A.; Brandstetter, M.; Lendl, B. Quantum cascade lasers (QCLs) in biomedical spectroscopy. *Chem. Soc. Rev.* **2017**, *46*, 5903–5924. [CrossRef]
25. Sroute, L.; Byrd, B.D.; Huffman, S.W. Classification of mosquitoes with infrared spectroscopy and partial least squares-discriminant analysis. *Appl. Spectrosc.* **2020**, *74*, 900–912. [CrossRef]
26. Khoshmanesh, A.; Christensen, D.; Perez-Guaita, D.; Iturbe-Ormaetxe, I.; O'Neill, S.L.; McNaughton, D.; Wood, B.R. Screening of wolbachia endosymbiont infection in aedes aegypti mosquitoes using attenuated total reflection mid-infrared spectroscopy. *Anal. Chem.* **2017**, *89*, 5285–5293. [CrossRef]
27. Schmid, M.; Rath, D.; Diebold, U. Why and How Savitzky–Golay Filters Should Be Replaced. *ACS Meas. Sci. Au* **2022**, *2*, 185–196. [CrossRef]
28. Müller, R.; Haertelt, M.; Niemasz, J.; Schwarz, K.; Daumer, V.; Flores, Y.V.; Ostendorf, R.; Rehm, R. Thermoelectrically-cooled inas/gasb type-ii superlattice detectors as an alternative to hgcdte in a real-time mid-infrared backscattering spectroscopy system. *Micromachines* **2020**, *11*, 1124. [CrossRef]
29. Galán-Freyle, N.J.; Pacheco-Londoño, L.C.; Román-Ospino, A.D.; Hernandez-Rivera, S.P. Applications of Quantum Cascade Laser Spectroscopy in the Analysis of Pharmaceutical Formulations. *Appl. Spectrosc.* **2016**, *70*, 1511–1519. [CrossRef]
30. Koyama, T.; Kino, S.; Sasaki, T.; Wada, Y.; Kasahara, R.; Oba, Y.; Matsuura, Y. Measurement and uniformization of power distribution on the prism for biomedical applications of mid-infrared, attenuated-total-reflection spectroscopy. In Proceedings of the Optical Fibers and Sensors for Medical Diagnostics, Treatment and Environmental Applications XXI, Online, 6–11 March 2021; Volume 11635, p. 41. [CrossRef]
31. Matsuura, Y.; Yoshioka, K.; Kino, S. Blood glucose measurement with multiple quantum cascade lasers using hollow-optical fiber-based ATR spectroscopy. In Proceedings of the Optical Fibers and Sensors for Medical Diagnostics and Treatment Applications XVIII, San Francisco, CA, USA, 27–28 January 2018; Volume 10488, p. 12. [CrossRef]
32. Song, L.; Han, Z.; Nie, H.; Lau, W.M. Compact Quantum Cascade Laser-Based Noninvasive Glucose Sensor Upgraded with Direct Comb Data-Mining. *Sensors* **2025**, *25*, 587. [CrossRef]
33. Román-Zas, C.; Ferreiro, B.; Terán-Baamonde, J.; Estela Del Castillo Busto, M.; Andrade, J.M.; Muniategui, S. Measurement of tyre-based microplastics using traditional and quantum cascade laser-based infrared spectrometry. *Spectrochim. Acta Part A Mol. Biomol. Spectrosc.* **2025**, *327*, 125321. [CrossRef]
34. Pazmiño-Betancourth, M.; Ochoa-Gutiérrez, V.; Ferguson, H.M.; González-Jiménez, M.; Wynne, K.; Baldini, F.; Childs, D. Evaluation of diffuse reflectance spectroscopy for predicting age, species, and cuticular resistance of Anopheles gambiae s.l under laboratory conditions. *Sci. Rep.* **2023**, *13*, 18499. [CrossRef]
35. Hugi, A.; Maulini, R.; Faist, J. External cavity quantum cascade laser. *Semicond. Sci. Technol.* **2010**, *25*, 083001. [CrossRef]
36. Lin, W.C.; Matcher, S.J. Swept-source OCT using pulsed mid-infrared light. In Proceedings of the Label-Free Biomedical Imaging and Sensing (LBIS), San Francisco, CA, USA, 4 March 2019; Volume 10890, p. 84. [CrossRef]
37. Omucheni, D.L.; Kaduki, K.A.; Mukabana, W.R. Rapid and Non-Destructive Identification of Anopheles Gambiae and Anopheles Arabiensis Mosquito Species Using Raman Spectroscopy via Machine Learning Classification Models. *Malar. J.* **2023**, *22*, 342. [CrossRef]
38. Omucheni, D.L.; Kaduki, K.A.; Mukabana, W.R. Identification of Three Medically Important Mosquito Species Using Raman Spectroscopy. *J. Raman Spectrosc.* **2023**, *54*, 512–523. [CrossRef]